Detecting, Visualizing, and Measuring Gold Nanoparticle Chirality Using Helical Pitch Measurements in Nematic Liquid Crystal Phases

Anshul Sharma,[†] Taizo Mori,[†,‡,§] Huey-Charn Lee,[⊥] Matthew Worden,[∥] Eric Bidwell,[∥] and Torsten Hegmann[*,†,⊥,∥]

[†]Liquid Crystal Institute, Chemical Physics Interdisciplinary Program, Kent State University, Kent, Ohio 44242, United States, [‡]World Premier International (WPI) Center for Materials Nanoarchitectonics (MANA), National Institute for Materials Science (NIMS), 1-1 Namiki, Tsukuba, Ibaraki 305-0044, Japan, [§]Japan Society for the Promotion of Science (JSPS), 5-3-1 Kojimachi, Chiyoda-ku, Tokyo 102-0083, Japan, [⊥]Department of Chemistry, University of Manitoba, Winnipeg, Manitoba, Canada R3T 2N2, and [∥]Department of Chemistry and Biochemistry, Kent State University, Kent, Ohio, 44242-0001 United States

ABSTRACT Chirality at the nanoscale, or more precisely, the chirality or chiroptical effects of chiral ligand-capped metal nanoparticles (NPs) is an intriguing and rapidly evolving field in nanomaterial research with promising applications in catalysis, metamaterials, and chiral sensing. The aim of this work was to seek out a system that not only allows the detection and understanding of NP chirality but also permits visualization of the extent of chirality transfer to a surrounding medium. The nematic liquid crystal phase is an ideal candidate, displaying characteristic defect texture changes upon doping with chiral additives. To test this, we synthesized chiral cholesterol-capped gold NPs and prepared well-dispersed mixtures in two nematic liquid crystal hosts. Induced circular dichroism spectropolarimetry and polarized light optical microscopy revealed that all three gold NPs induce chiral nematic phases, and that those synthesized in the presence of a chiral bias (disulfide) are more powerful chiral inducers than those where the NP was formed in the absence of a chiral bias (prepared by conjugation of a chiral silane to preformed NPs). Helical pitch data here visually show a clear dependence on the NP size and the number of chiral ligands bound to the NP surface, thereby supporting earlier experimental and theoretical data that smaller metal NPs made in the presence of a chiral bias are stronger chiral inducers.

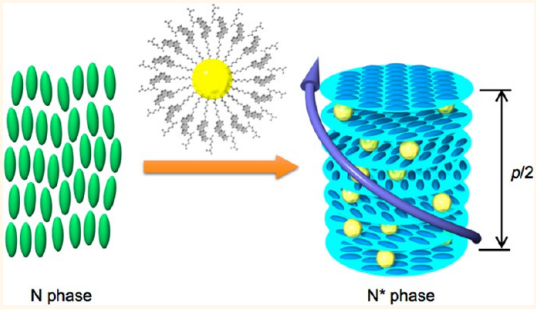

KEYWORDS: nanoparticles · chirality · helical pitch · liquid crystals

Over the last two decades scientists and engineers have very elegantly combined NPs and chiral molecules[1] to generate materials that have unique applications as biological probes and sensors,[2,3] for stereoselective separations and catalysis,[4,5] in liquid crystals (LCs),[6−9] and show great potential in nonlinear optics and metamaterials with negative index of refraction.[10,11] There are two ways by which chiral optical nanomaterials can be obtained: (a) by colloidal chemical synthesis[12−15] and (b) by assembly of NPs to generate 3-D arrangements assisted by chiral templates.[16−18] It is the optical activity that makes these metamaterials so unique. Three main mechanisms have been proposed and explored to understand the optical activity of chiral ligand capped NPs: (I) an intrinsically chiral metal core;[19] (II) a dissymmetric field model (*i.e.*, an achiral core is influenced by the vicinal effect or electrostatic interactions of the chiral adsorbate); and (III) a chiral footprint model in which the core is achiral but the arrangement of the attached ligands generates optical activity.[12,20−22] Recent research has seen significant attention to well formed metal clusters and NPs[23−26] within a size regime of 2−10 nm due to their enhanced optical activity. For the most stable clusters (Au_{25}), it has been found that *in situ* preparation of such clusters in the presence of a chiral ligand enhances the optical activity compared to clusters formed *via* ligand exchange.[23,27,28] Recent reviews by Bürgi,[12]

* Address correspondence to thegmann@kent.edu.

Received for review September 3, 2014 and accepted November 10, 2014.

Published online November 10, 2014
10.1021/nn504980w

© 2014 American Chemical Society

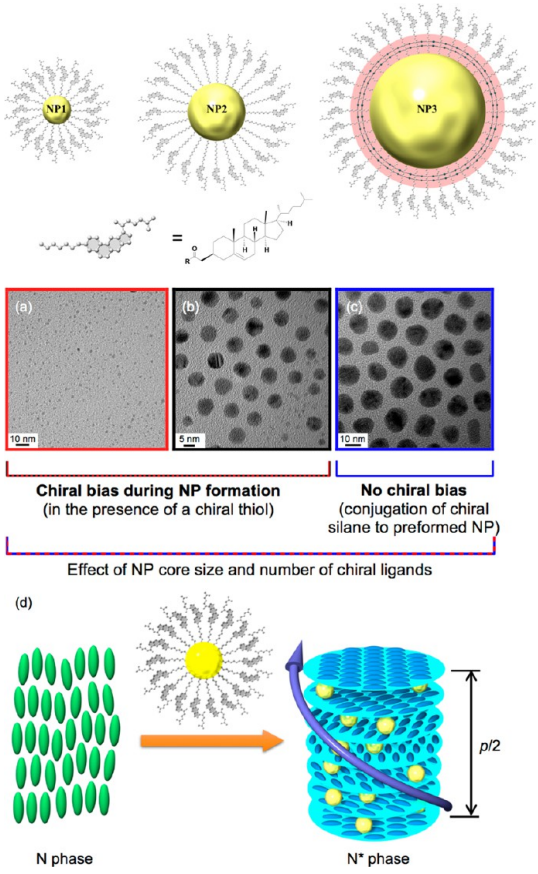

Figure 1. High-resolution TEM images of (a) NP1 (1.77 ± 0.11 nm), (b) NP2 (5.54 ± 1.23 nm), and (c) NP3 (10.09 ± 2.72 nm) shown above. (d) Cartoon introducing the concept of using nematic liquid crystal phases to detect, visualize, and measure the chirality of chiral ligand-capped NPs using helical pitch measurements.

Garzón,[20] Liz-Marzán,[29] and Tang *et al.*[30] provide useful overviews on the origin of chirality in both metal clusters and NPs.

It has been shown that introducing chiral dopants into achiral liquid crystal hosts can transform them into chiral condensed phases with unique optical properties and a wide range of applications.[31,32] In search of an ideal system to sense and quantify chirality of chiral ligand capped metal NPs, we have verified that chiral, thiol-functionalized gold NPs can successfully transfer chirality to achiral nematic (N) LCs.[6,7] These NPs were capped with (*S*)-naproxen, a chiral nonsteroidal anti-inflammatory drug known to induce chiral nematic (N*) phases. While these NPs appeared to outperform the pure organic (*S*)-naproxen as a chiral dopant, the limited miscibility of these gold NPs in N-LC hosts prohibited a quantification of their chiral induction strength.

To overcome this limitation, the aim of the current work was to qualitatively measure and understand the effectiveness of chirality transfer of in situ capped gold NPs (presence of chiral bias during NP formation) compared with those obtained by chiral ligand conjugation to existing NPs (the chirality is "installed" after NP formation). We also probed the role of size and number of chiral ligands (Figure 1). The selection of a chiral liquid crystalline (mesogenic) ligand, highly compatible with N-LC hosts, should allow us to quantify the effectiveness of chirality transfer using established methods for characterizing N-LCs (*i.e.*, helical pitch measurements).[31,33] Cholesterol was chosen as the chiral LC ligand not only for its compatibility with N-LCs but also because of its importance to biological systems such as bilayer membranes,[34] as general building block for LC applications such as thermal sensors,[35] and as gelator.[36] We started with the synthesis of cholesterol-thiolate functionalized gold NPs (**NP1** and **NP2**), made in the presence of a chiral bias, and cholesterol conjugated NPs (**NP3**) obtained *via* silane conjugation to MPS-coated (MPS, (3-mercaptopropyl)trimethoxysilane) NPs with no chiral bias present during NP growth.

We then investigated the chirality transfer from the well-dispersed NPs (**NP1** – **NP3**) in two LC hosts (in the nematic phase of LC1 and LC2, Scheme 1) first by induced circular dichroism (ICD) spectropolarimetry in thin films followed by helical pitch measurements using the Cano wedge method to calculate the helical twisting power, HTP (β_M, a measure for the ability of a chiral dopant to twist a nematic LC phase).

$$\beta_M = 1/p \cdot c \qquad (1)$$

where p is the helical pitch and c is the concentration of the chiral dopant.

RESULTS AND DISCUSSION

Characterization. The synthesis of all intermediates and chiral ligands was accomplished according to previously reported methods. The synthetic details, analytical data, as well as UV–vis and CD spectra can be found in the Supporting Information (see Figures S1 and S2). The purified gold NPs were first characterized by UV–vis spectroscopy (Supporting Information Figure S3) and high-resolution transmission electron microscopy (HR-TEM in Figure 1). Supporting Information Figure S3 shows the visible absorption spectrum (400–800 nm) in toluene for **NP1**, **NP2** and **NP3**. **NP1** did not show any surface plasmon resonance (SPR) peak (Supporting Information Figure S3a), which confirms that these particles are smaller than 5 nm in diameter as seen by TEM (Figure 1a).[37] A characteristic SPR band was observed for both **NP2** (λ_{max} = 529 nm) and **NP3** (λ_{max} = 531 nm) as shown in Supporting Information Figure S3, panels b and c, respectively. The change in wavelength of the SPR band maximum of **NP2** and **NP3** is due to increase in size as evident from TEM images (Figure 1b,c).[38]

The average size distribution obtained from the TEM image analysis is presented in Table 1. The purity and functionalization of the obtained gold NPs was

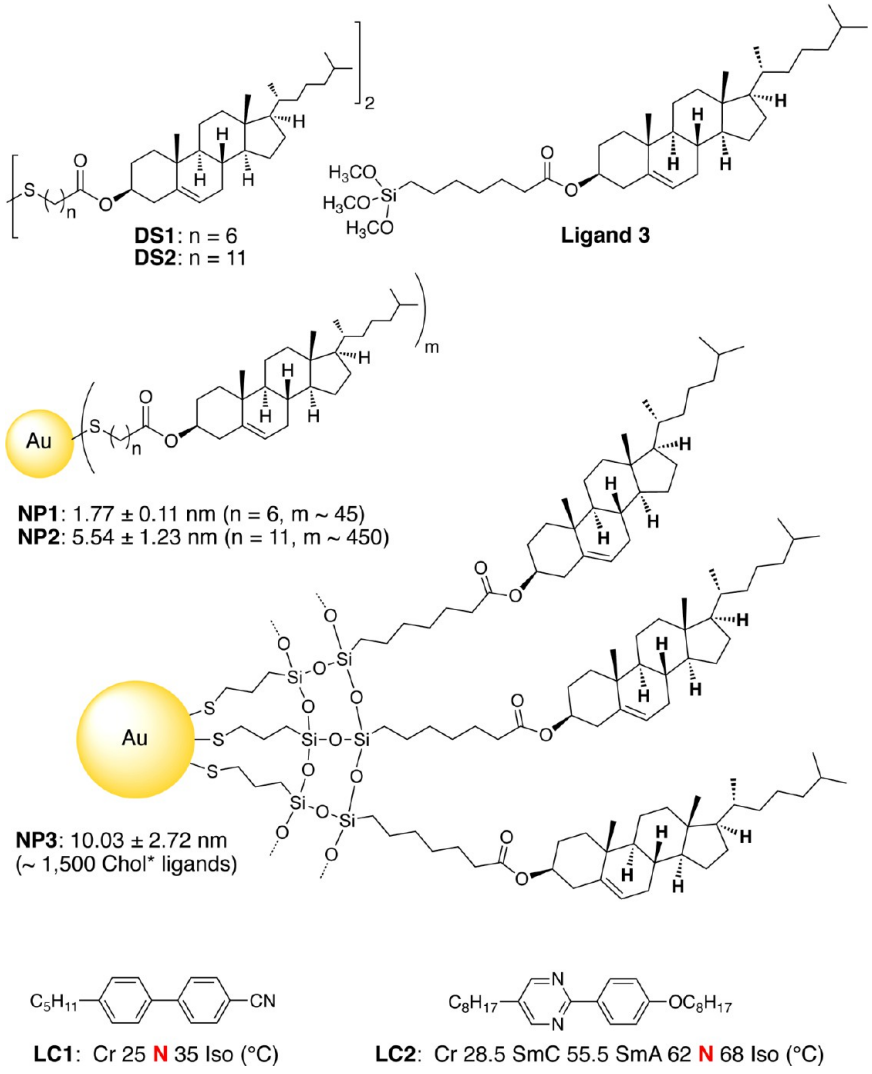

Scheme 1. Chemical structure of DS1, DS2, ligand 3, and NP1−NP3, as well as structure and phase sequences of LC1 and LC2.

TABLE 1. Average NP Core Diameter (nm), Number of Au Atoms, Number of Ligands, and Average Molecular Weight (M_w) of NP1, NP2, and NP3

NP	NP core diameter (nm)[a]	number of Au atoms	number of ligands	average M_w of NPs[b]
NP1	1.77 ± 0.11	170	45	57380
NP2	5.54 ± 1.23	5234	450	1295300
NP3	10.09 ± 2.72	31622	1493	7356700

[a] TEM image analysis of more then 100 NPs was performed using ImageJ. [b] Average molecular weight (M_w) of NPs was calculated assuming a hexagonal close-packed gold NPs. For detailed calculations see Supporting Information.

confirmed by ^{1}H NMR spectroscopy (see Figures A1 to A11 for all ^{1}H NMR spectra of intermediates and NPs in the appendix of the Supporting Information). The ^{1}H NMR spectra show characteristic broadened resonance peaks and no indication of free, nonbound thiols for **NP1** and **NP2** or free thiols and silanes for **NP3**.[39] Assuming a spherical shape for the NPs (which at this size provides similar numbers as assuming a polyhedral shape), we also calculated the average molecular weight of each NP according to the model developed by Gelbart *et al.*[40] The results from these calculations for all three NPs (**NP1**−**NP3**) including molecular weight, number of gold atoms, and number of organic ligands on the NP surface are collected in the Supporting Information (page S10). This allows us to calculate the average and number of organic ligands present in a given LC-NP mixtures (see Supporting Information Table S1). We will use this data later to compare the effectiveness to induce an N* phase among the three NPs and between NPs and free chiral ligands (such as the disulfides **DS1** and **DS2** used for the synthesis of **NP1** and **NP2**, respectively, and **ligand 3** used for the synthesis of **NP3**).

Optical Activity and Circular Dichroism. For an initial understanding of the optical activity of **NP1**, **NP2**, and **NP3**, CD spectra were measured in $CHCl_3$ solutions (Supporting Information Figure S4). We also measured CD spectra of all intermediate compounds (**1**−**5**), both disulfide 1 (**DS1**) and 2 (**DS2**), as well as **ligand 3** (Supporting Information Figure S2) in solution. All

organic compounds showed CD bands with negative Cotton effect and absorbance in the UV region. The NPs synthesized or formed in the presence of a chiral thiol (**NP1** and **NP2**) showed negative CD signals. **NP1** (Supporting Information Figure S4a), being the smallest in size and with the shorter hydrocarbon spacer between the cholesterol core and the NP surface (C6), showed only a weak CD peak around 343 nm where the free organic ligand (**DS1**) does not absorb light (Supporting Information Figure S2e), and no CD at longer wavelength (no plasmonic CD). Kim *et al.* reported the observations of such CD spectra for D- and L-Pen (penicillamine)-capped gold NPs with similar NP core diameter (1.99 ± 0.3 nm). A CD response was found at wavelengths where the free ligands (D-Pen or L-Pen) do not absorb.[2] Hence, these CD responses could be linked to interband metal and ligand-to-metal charge transfer transitions.[41−43] In case of **NP2**, which is slightly larger in core diameter compared to **NP1**, CD signals at the wavelength of the SPR band (plasmonic CD) along with additional CD bands at 573 and 649 nm were observed (Supporting Information Figure S4b). A possible explanation for this behavior can be given considering the optical coupling between NPs and chiral adsorbates due to Coulomb interactions and possible plasmon field enhancement.[44,45] Govorov *et al.*[46] studied quasi-spherical gold NPs (>20 nm) conjugated with oligonucleotides to elucidate this mechanism and compared the CD results with those for nonplasmonic quantum dots. For the case of gold NPs, an enhancement of CD band intensity was observed at their SPR wavelength only when the chiral oligonucleotides were attached. No plasmonic CD signal was seen when the same experiment was repeated with a quantum dot in place of the gold NP.[47] Similar data were collected for our synthesized NPs, which also showed enhanced CD signals at the SPR band wavelength.

To study the effect of a chiral bias during the formation of NPs we synthesized NPs coated with the same cholesterol chiral moiety but formed in absence of a chiral bias. **NP3** synthesized first *via* ligand exchange (surfactant CTAB for MPS) followed by silane conjugation to MPS-coated NPs showed a broad negative CD band (see Supporting Information Figure S4c). Bürgi *et al.*[27,48] and others[49,50] performed extensive studies on ligand exchange reactions of intrinsically chiral Au_{25}, Au_{38} and Au_{40} clusters. Bürgi *et al.* showed that ligand exchange forms mixtures of clusters that are pairs of enantiomers and diastereomers.[26] Assuming that place exchange reactions are nondiastereoselective and that both enantiomers react at the same rate, these species will cancel out each other's effect and will not have any contribution to the net optical activity. In a case where the ligand exchange reaction has different rate constants for each enantiomer then the expected CD spectra would be the sum of optical activity of four different species. The latter could explain the observation of broad, undefined CD peaks in regions of both UV as well plasmonic wavelengths in **NP3**. However, it is important to mention here that our NPs are not well-defined clusters and that several effects will average out. Nevertheless, the solution CD data indicate that the presence of chiral ligands during the formation of NPs critically influences the electronic structures of the metal NP cores (*i.e.*, chiral gold NP surface—more pronounced for smaller metal **NP1**).

To test the effectiveness of chirality transfer of the synthesized NPs to achiral liquid crystal hosts, we executed careful thin film ICD experiments for the LC-NP mixtures. To avoid CD reflection bands, we only tested the lowest concentration of NPs in the LC hosts.[7] Samples were rotated at intervals of 45° to cancel out contributions of linear dichroism and birefringence.[51] Even in very thin film samples it is not trivial to avoid possible saturation of the absorbance of the CD signal at the detector. So only results based on the sign, and not the intensity, of the CD signals are discussed. As expected, for 0.5 wt % of **NP1** (Supporting Information Figure S5a) and **NP2** (Supporting Information Figure S5c) in LC1 at 30 °C the sign of the CD bands is always negative, leading to sum negative CD signals (Supporting Information Figure S5b,d). These thin films between quartz substrates were also studied using polarized light optical microscopy (POM). For LC1 doped with **NP1** or **NP2** at 0.5 wt %, characteristic chiral finger textures were observed between crossed polarizers (see Figure 2, panels b and d, respectively). However, in the case of **NP3**, CD spectra collected at different sample rotation angles showed both negative and positive signs leading to a net zero CD signal (sum of all spectra). Upon observation under POM, this sample showed marble-type textures typical for N-LCs. Similar CD results for all three NPs were also found for mixtures with 0.5 wt % in the N phase of LC2 at 66 °C (Supporting Information Figure S6), which shows that these effects are not host specific. The POM images of LC2 doped with the NPs corroborate these ICD results, with **NP1** and **NP2** in LC2 again showing cholesteric finger textures characteristic for N* phases (Supporting Information Figure S8j,k) and LC2 doped with **NP3** showing a *Schlieren* texture typical for an N-LC phase (Supporting Information Figure S8i).

Texture Analysis and Chirality Transfer. The texture observation between untreated quartz discs indicated that the current NPs disperse well in the N phase of both LC hosts (no obvious sign of aggregation). They also show that simple analysis of textures characteristic for N or N* phases by POM between crossed polarizers can be used to discriminate between chiral and achiral mixtures (or "weakly chiral" – *i.e.* too low concentration of chiral NPs or inefficient chirality transfer). All mixtures of **NP1**-**NP3** in LC1 and LC2 were prepared

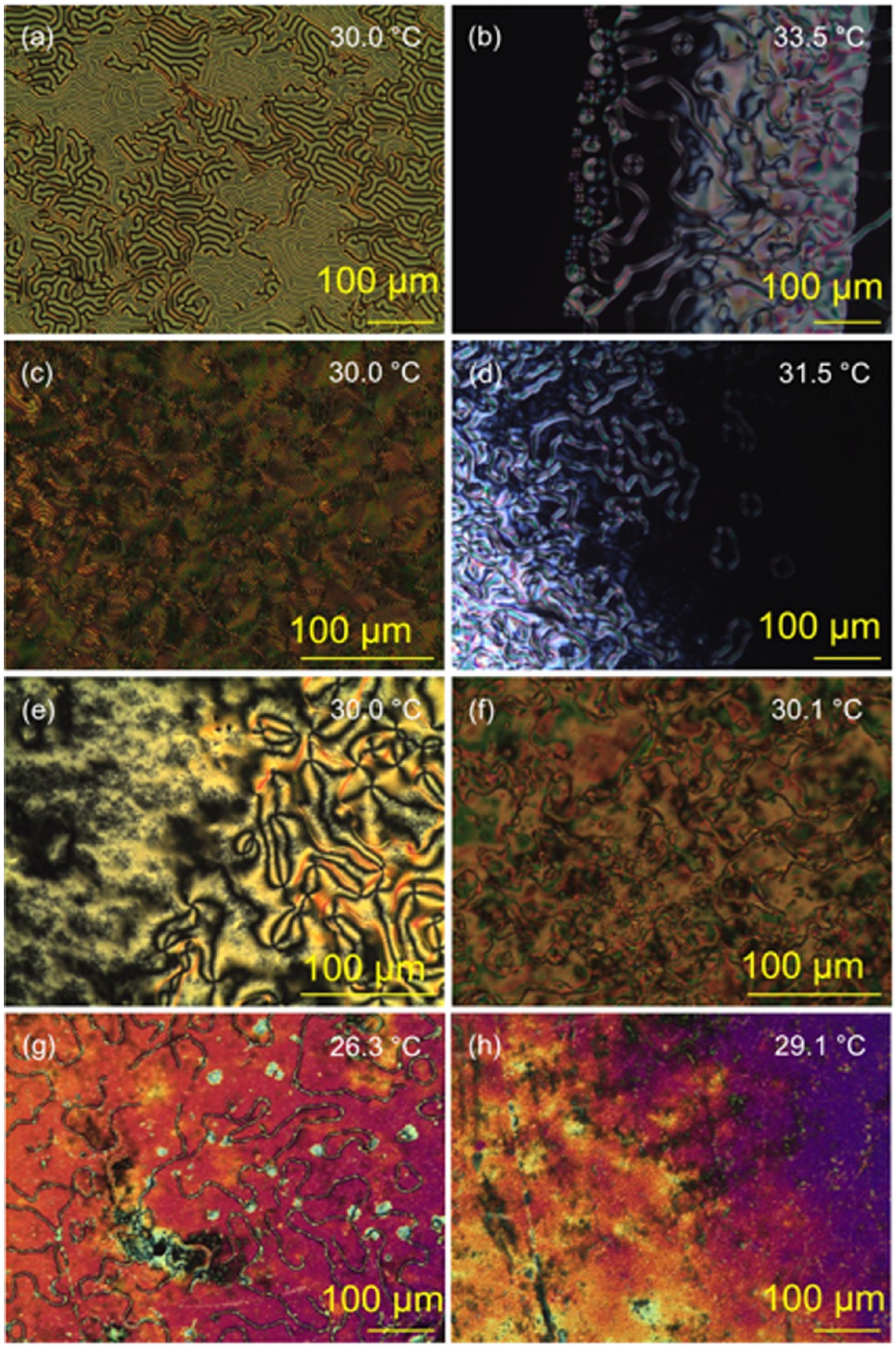

Figure 2. Polarized light optical microscopy (POM) micrographs (90° crossed polarizers) of LC1 doped with (a) NP1 (5 wt %, untreated glass slides), (b) NP1 (0.5 wt %, quartz cell), (c) NP2 (5 wt %, untreated glass slides), (d) NP2 (0.5 wt %, quartz cell), (e) NP3 (5 wt %, untreated glass slides), (f) NP3 (0.5 wt %, quartz cell), (g) DS1 (0.03 wt %, untreated glass slides), and (h) DS1 (0.03 wt %, quartz cell).

following protocols previously established in our laboratory.[6,52] LC1 was chosen as host to allow us to compare the results with our previous findings on chirality transfer to an achiral LC host.[6,7] LC2 was used to see if the same NP would transfer chirality to structurally dissimilar LC hosts. Earlier studies in our group have shown that the effective range of NP doping in LC hosts lies between 0.5 and 5 wt %.[53−56] Considering this, we prepared 0.5, 2.5, and 5 wt % **NP1**, **NP2**, and **NP3** mixtures in LC1 and LC2. For comparison, we also analyzed neat **DS1**, **DS2** and **ligand 3** as well as mixtures of **DS1**, **DS2** and **ligand 3** at the same concentrations (w/w) in LC1 and LC2. All mixtures were first observed under POM (crossed polarizers) between cleaned, untreated glass slides. Neat **DS1**, **DS2** and **ligand 3** on cooling from the isotropic liquid phase

showed focal conic fan textures typical for unaligned N* phases at 122.0 °C (Supporting Information Figure S7a), 107.0 °C (Supporting Information Figure S7b) and 25.8 °C, respectively (Supporting Information Figure S7g). Mixtures with 5 wt % of **DS1** (Supporting Information Figure S7e), **DS2** (Supporting Information Figure S7f) and **ligand 3** in LC1 (Supporting Information Figure S7h) showed rather similar cholesteric finger textures, at the same temperature on cooling (with a perceivable slight increase in the distance between birefringent stripes from **DS1** over **DS2** to **ligand 3**, frequently indicative of an increase in the helical pitch). Considering the similarity of these three textures and a similar temperature dependence of the helical pitch, all three ligands could be considered quite comparable chiral additives. In homeotropic cells (helix axis parallel to the substrates), **DS1** at 0.5 and 5 wt % (Supporting Information Figure S10a,b) in LC1 remained optically black (the helical pitch is too large to show fingerprint textures), whereas **DS2** at 5 wt % (Supporting Information Figure S10d) in LC1 starts showing a typical fingerprint texture. **Ligand 3** in LC1 in homeotropic cells both at 0.5 wt % (Supporting Information Figure S10e) and 5 wt % (Supporting Information Figure S10f) in LC1 showed typical fingerprint textures.

POM textures observed between untreated glass slides provided the first insights in the mesomorphic behavior (*i.e.*, effectiveness of chiral induction) of **NP1**−**NP3** in mixtures with both LC1 and LC2. For the lowest concentration of 0.5 wt % of **NP1** (Supporting Information Figure S8a) and **NP2** (Supporting Information Figure S8b) in LC1 between untreated glass slides *Schlieren* textures common for N-LC phases (or N* phases with large helical pitch of several tens of microns) were observed. None of the current textures showed birefringent stripes as textures previously observed by our group for LC-NP mixtures (as a result of segregation of NPs to the glass-LC interfaces accompanied by the formation of π-walls),[6,53] and would here rather indicate that the NPs are well dispersed and do not aggregate or segregate. Another indication of this is the sharp phase transition from the isotropic liquid to the N-LC phase, which is stabilized by about 1−2 °C rather than destabilized.[56]

On further increasing the concentration to 5 wt % of **NP1** (Figure 2a) and **NP2** (Figure 2c) in LC1, we observed typical fingerprint textures corresponding to an N* phase of the host LC. Conversely, in the case of **NP3** doped in LC1 or LC2 at both 0.5 wt % (Supporting Information Figure S8c) and 5 wt % (Figure 2e), *Schlieren* and marble textures typical for N-LC phases were found.

Mixtures of **NP1** and **NP2** at 0.5 and 5 wt % in LC2 also showed fingerprint, cholesteric finger, and focal conic fan textures characteristic for N* phases (Supporting Information Figure S8d−h). **NP3** at 0.5 and 5 wt % in LC2 (Supporting Information Figure S8f,i), however, showed textures similar to chiral finger textures indicating a larger helical pitch in comparison to **NP1** or **NP2** in LC2. The chiral induction not seen for LC1 is likely the result of the better miscibility of **NP3** in LC2 in comparison to the polar LC1 not flanked by two hydrocarbon tails. These preliminary observations confirmed our speculation that gold NPs formed in the presence of a chiral bias are more efficient chiral inducers than NPs formed in absence of a chiral bias in N-LC hosts. For a better comparison of an observable helical pitch of the induced N* phase in LC1 and LC2, all LC-NP mixtures were also observed under POM between glass slides treated to induce homeotropic boundary conditions. For both **NP1** and **NP2** at the lowest concentration of 0.5 wt %, homeotropic textures were observed (Supporting Information Figure S9a,b, helical pitch of several tens of micron).

TABLE 2. Helical Pitch (p) Values (μm)[a] of NP1−NP3 and DS1, DS2, and ligand 3 Depending on the Concentration (w/w) of the NPs in LC1

wt % of NPs	2.5	5	10
mixture		helical pitch (p)/μm	
NP1 + LC1	11.18 ± 0.71	6.23 ± 0.50	2.65 ± 0.15
NP2 + LC1	6.89 ± 0.06	5.33 ± 0.69	2.45 ± 0.07
NP3 + LC1	—[b]	—[b]	—[c]
DS1 + LC1	—[d]	4.09 ± 0.07	—[d]
DS2 + LC1	—[d]	4.07 ± 0.04	—[d]
3 + LC1	—[d]	7.11 ± 0.37	—[d]

[a] Value ± standard deviation from three independent wedge cell measurements. [b] At these concentrations of **NP3** in LC1 or LC2, no helical pitch could be measured in wedge cells (p is too large, see Figure 3d). [c] The larger **NP3** particles did show signs of aggregation at this high weight % (*i.e.*, volume fraction). [d] For a comparison between NPs and organic ligands, only the 5 wt % mixtures were needed and measured.

As observed by POM between untreated glass slides, cholesteric finger or fingerprint textures indicative of an N* phase began to appear at concentrations as low as 2.5 wt % of **NP1** or **NP2** in LC1. The thin films eventually displayed archetypal fingerprint textures on increasing the concentration of **NP1** and **NP2** in LC1 to 5 and 10 wt % (Supporting Information Figure S9c−h).

Helical Twisting Power (HTP). To quantify the efficiency of chirality transfer from the chiral ligand capped NPs to the N-LC hosts, we used a well-established method to measure the helical pitch (p) and calculate the helical twisting power, HTP (β_M).[33,57] First, all NP-LC mixtures were heated to the isotropic liquid phase and then filled in wedge cells. After slowly cooling the samples below the Iso/N* phase transition, we observed the test cells under POM. For comparison, we also tested **DS1**, **DS2** and **ligand 3** at 5 wt % in LC1. The p values for **DS1**, **DS2** and **ligand 3** were found to be 4.09, 4.07, and 7.11 μm, respectively, as expected from the prior POM studies.

The helical pitch values for **NP1**, **NP2**, and **NP3** depending on the NP concentration in LC1 as well as

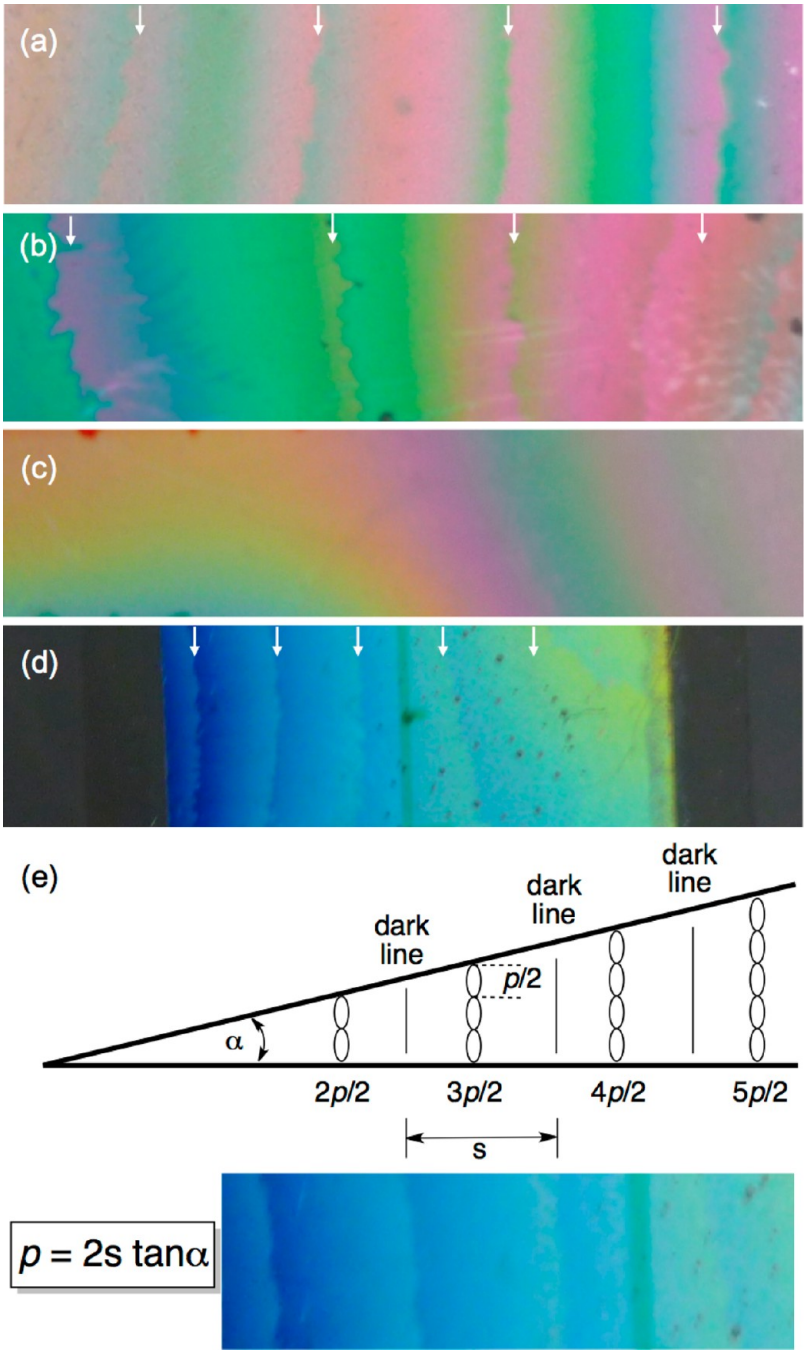

Figure 3. Images of Grandjean-Cano wedge cells (crossed polarizers) showing Grandjean steps (lines) of the induced N* phase of LC1 after doping with (a) 5 wt % of NP1, (b) 5 wt % of NP2, and (c) 5 wt % of NP3 (showing no evidence for Grandjean steps), and (d) 10 wt % of NP1. (e) Grandjean-Cano wedge cell method to determine the helical pitch (*p*) of an N* phase (*s* = distance between two disclination lines).

the values for the 5 wt % of **DS1**, **DS2**, and **ligand 3** are summarized in Table 2. The corresponding wedge cell images are collected in Figures 3 and 4 (larger versions of more concentrations in Supporting Information Figure S11). At the same weight concentration (5 wt %) in LC1, **NP1** and **NP2** both showed only slightly larger helical pitch value of 6.23 and 5.33 μm as compared to **DS1** and **DS2**. These values are comparable to previously reported values for chiral binaphthalene derivatives in LC1.[58] For 5 wt % of **NP3** in LC1 no defect (Grandjean) lines were detected, indicating that the helical pitch is very (too) large. For the HTP values calculated using eq 1, we obtained greatly elevated values for **NP1** and **NP2** compared to **DS1** and **DS2**. For 5 wt % of **DS1** and **DS2** (using mol % to compare the HTP based on the number of chiral molecules in the mixture, while neglecting any contributions from the apparent chirality of the NP), HTP values of 19.70 and 22.31 μm^{-1} were calculated, respectively. Since the calculation of the HTP (using mol faction rather

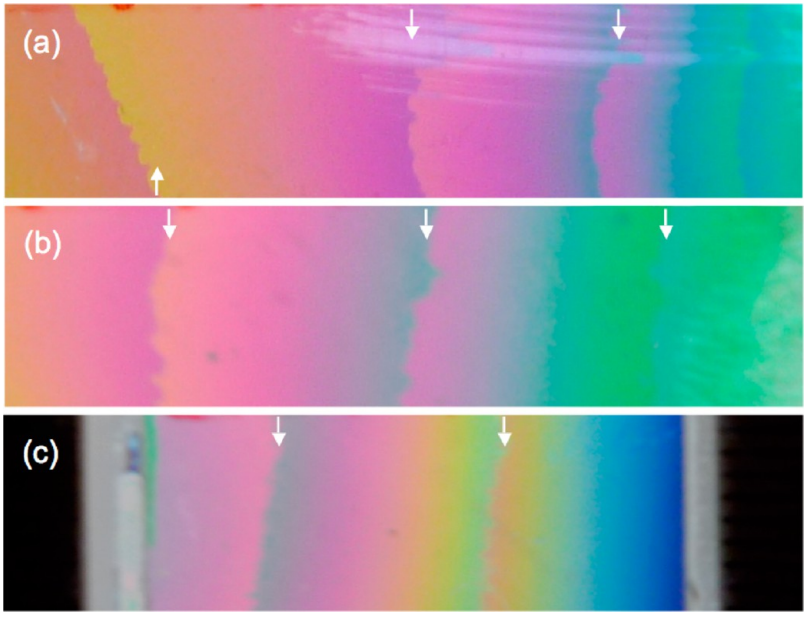

Figure 4. Images of Grandjean-Cano wedge cells (crossed polarizers) showing Grandjean steps (lines) of the induced N* phase of LC1 after doping with 5 wt % of (a) DS1, (b) DS2, and (c) ligand 3.

then wt %, *vide supra*) is based on the molecular weight of the chiral additive (see Table 1), significantly larger values are obtained for both NPs. For the HTP values of **NP1** and **NP2**, we calculated 1522.1 and 91801.1 μm^{-1}, respectively. Chen and co-workers reported a related comparison of HTP values between chiral LC polymers and their low molar mass counterparts.[59] By comparing the amount of chiral ligand present (*i.e.*, standardizing the HTP values based on the amount of chiral molecules in each mixture), we found that the **NP1**–LC1 and **DS1**–LC1 mixtures had similar helical pitch values, despite the **NP1**–LC1 containing two to 3 orders of magnitude fewer chiral ligand molecules than the **DS1**–LC1 mixture at the same wt % (*e.g.*, 0.5 or 5 wt %, entry 1 and 2 in Supporting Information Table S1).

This indicates that for a meaningful comparison on the efficiency to induce an N* phase in achiral N-LC hosts we need to compare mixtures with the same amount of chiral ligand molecules present at a given concentration in LC1. To do so, we prepared a mixture of 0.03 wt % **DS1** in LC1 (identical mol % of chiral ligands as 5 wt % **NP1** in LC1, Supporting Information Table S2), and, as expected, no chiral textures were observed by POM (Figure 2g,h) since the concentration of **DS1** in LC1 was too low. The concentration with same number of chiral molecules (ligands) of **DS2** in LC1 as for **NP2** in LC1 is again almost 2 orders of magnitude smaller (9.6×10^{-4} wt % of **DS2** match 5 wt % of **NP2** in LC1). These calculations clearly indicate that the chiral ligand-capped gold NPs are more efficient chiral dopants than their free chiral ligand counterparts. The data also show that NPs made in the presence of a chiral bias (**NP1** and **NP2**) are more efficient chiral dopants than NPs made in the absence of a chiral bias during NP formation (**NP3**). Comparing **NP1** and **NP2** at same pitch value (*e.g.*, 2.70 μm, obtained from Supporting Information Figure S12) in the same host LC1 at the same composition (9.53 wt %), we find that the mixture of **NP1** in LC1 contains 1 order of magnitude fewer chiral ligands than **NP2** in LC1 (Supporting Information Table S2). Hence, in order to reveal which NP is the most efficient chiral dopant we might want to compare mixtures that contain the same number of chiral ligand molecules in LC1. What we find is this: To reach the same mole fraction of chiral ligand as 5 wt % **NP1** in LC1 (and the same helical pitch or HTP), we would need to add and disperse 69.9 wt % of **NP2** in LC1. In the case of **NP3**, 14.5 wt % of **NP1** or 88.55 wt % of **NP2** would be needed to obtain a mixture with same mole fraction of chiral ligand as 5 wt % of **NP3** in LC1.

One might theoretically be able to achieve the same helical pitch value, but at such high NP weight fractions the NP would severely aggregate and then segregate to the interfaces between the N-LC and both substrates, which would result in homeotropic alignment of the N-LC as described in our previous work.[6,60] Nevertheless, we cannot entirely ignore in this discussion that **NP2** in LC1 induces a tighter helical pitch than **NP1** in LC1 despite the lower overall number of chiral ligands. **NP2** featuring surface plasmon CD signals (**NP1** does not) could be considered the more efficient chiral inducer in N-LC phases based on the weight fraction in LC1 (Table 2). While there are fewer NPs in the **NP2**–LC1 mixture in comparison to the **NP1**–LC1 mixture, the volume fraction of **NP2** in LC1 is slightly higher considering NP core volumes of ~3 and ~90 nm^3 for **NP1** and **NP2**, respectively (see Supporting

Information Table S3 for the number of NPs in the 0.5 and 5 wt % mixtures).

CONCLUSIONS

We have demonstrated the important role NP size and the presence or absence of a chiral bias during NP formation play in chiroptical activity of chiral ligand-capped gold NPs. Our findings illustrate that interactions between N-LC phases and chiral ligand-capped gold NPs can serve as a unique platform to carefully study, sense, and quantify NP chirality using well-established methods to detect chirality in N-LCs. The LC-NP system described here only hints at the number of possibilities that research in this area could explore to better understand and apply NP chirality. Such possibilities include, but are not limited to, changing the NP shape (*e.g.*, nanorods with more intense plasmonic CD signals and higher chiral anisotropy factors, g, defined as $g = \Delta\varepsilon/\varepsilon$, with ε as the isotropic extinction coefficient and $\Delta\varepsilon$ the difference in ε of left and right circularly polarized light) or adjusting the NP synthesis to get stable, well-defined clusters. A great opportunity also lies in the use of lyotropic chromonic LC phases, where hydrated assemblies of nonamphiphilic molecules (forming stacks) could be influenced in a chiral environment created by most of the hydrophilic, chiral ligand-capped metal NPs described by other groups. Recent data suggest that chiral interactions between such chromonic LC stacks can cross a 6 nm separation[61] (the size of many metal NP systems) leading to bulk N* phases with typical fingerprint textures. A recently discovered LC system even more sensitive to chirality is the lyotropic chiral smectic-C* phase described by Giesselmann and co-workers.[62] Here, both the helical pitch of typical fingerprint textures and the occurrence of a measurable spontaneous polarization (that is highly sensitive to chirality) could be used to detect and quantify metal NP chirality.

Though there are still open questions about possible contributions of NP core or surface chirality, we clearly demonstrated that the presence of a chiral bias during the NP formation produces gold NPs that induce more prominent, stronger chiral effects in condensed N-LC phases in comparison to NPs synthesized in the absence of a chiral bias. We also showed that smaller gold NPs with an overall lower number of chiral ligands attached to the NP surface in the N-LC mixture outperform larger gold NPs. The key finding, however, is that NP chirality can be transmitted to and sensed by N-LC phases, which, in turn, permitted us to image and measure the extent of gold NP chirality transfer. We believe that these studies have tremendous implications for the use of metal NPs as chiral catalysts, chiral discriminators, and chiral metamaterials.

EXPERIMENTAL SECTION

Synthesis. All compounds and NPs were synthesized according to Supporting Information Schemes S1 and S2. For detailed synthetic information and ^{1}H NMR spectra of reaction intermediates **1**−**5**, the disulfides **DS1** and **DS2**, **ligand 3**, the CTAB-capped NPs as well as **NP1**, **NP2** and **NP3** see the Supporting Information. The purified NPs were characterized by ^{1}H NMR spectroscopy, HR-TEM analysis/imaging, CD spectropolarimetry, and UV−vis spectrophotometry. The average size of the gold NPs as determined by HR-TEM imaging and image analysis is summarized in Table 1 (for HR-TEM images see Figure 1).

LC-NP Composites. All NP-LC mixtures were prepared by mixing exactly weighed amounts of solid LC and NPs. From 0.5 wt % up to 10 wt % of **NP1**, **NP2** and **NP3** in LC1 or LC2 were then mixed in chloroform by stirring and sonication. Thereafter, the solvent was completely evaporated under a stream of dry nitrogen at a temperature above the N/Iso phase transition temperature of the LC material, *i.e.* at 45 °C for LC1 and 70 °C at LC2 for 24 h. The obtained mixtures were finally subjected to pulsed sonication using a sonotrode at in the isotropic phase of LC for several seconds.

Sample Preparation for CD, POM and Pitch Measurements. For the CD measurements, thin films of the LC-NPs mixtures were prepared between two precleaned quartz substrates (square, 19 × 19 × 0.5 mm; and disc, 1 in. × 1/16 in.) separated by 10-μm fiberglass spacers. The cell gaps of these cells were measured following an established protocol.[57] Cells inducing homeotropic alignment[63] and wedge cells for helical pitch measurements[57] were made following well-known methods described previously by Palffy-Muhoray and co-workers. To validate this method to calculate helical pitch and HTP prior to applying it to the current NP-LC mixtures, we tested a known chiral dopant[64,65] (R811, 4 wt %) in LC1. The pitch value was found to be 1.95 μm and an HTP value of 0.128 μm wt %$^{-1}$ (as compared to 0.14 μm wt %$^{-1}$ given in ref 65).

Conflict of Interest: The authors declare no competing financial interest.

Supporting Information Available: These include synthetic details, synthesis schemes, all calculations for the used NPs, UV−vis, CD as well as NMR spectra, and POM images (including larger versions of those used in the main text). This material is available free of charge *via* the Internet at http://pubs.acs.org.

Acknowledgment. A.S. performed most syntheses, characterization and testing of the materials, H.C.L. and E.B. assisted with the synthesis of key intermediates, T.M. assisted with collecting and interpreting CD data, and M.W. performed all TEM measurements. T.H. designed and directed the research. A.S., T.M., and T.H. drafted the manuscript. The authors would like to thank Dr. L.C. Chien and A. Varanytsia for their help with cell gap measurements. This work was supported by the Ohio Third Frontier (OTF) program for Ohio Research Scholars "Research Cluster on Surfaces in Advanced Materials" (support for TH), which also supports the cryo-TEM facility at the Liquid Crystal Institute (Kent State University), where current TEM data were acquired. Finally, T.M. acknowledges financial support (postdoctoral scholarship) from the Japan Society for the Promotion of Science (JSPS), and HCL for a graduate internship from the Canadian Commonwealth Scholarship Program (CCSP). Funding sources for this study were Ohio Third Frontier Program (OTF), Natural Sciences and Engineering Research Council of Canada (NSERC), Canada Foundation for Innovation (CFI), Japan Society for the Promotion of Science (JSPS).

REFERENCES AND NOTES

1. Amabilino, D. B., Ed.; In *Chirality at the Nanoscale*; Wiley-VCH Verlag GmbH & Co. KGaA: Weinheim, 2009; p XXII.
2. Kang, Y.; Oh, J.; Kim, Y.; Kim, J. S.; Kim, H. Chiral Gold Nanoparticle-Based Electrochemical Sensor for Enantioselective Recognition of 3,4-Dihydroxyphenylalanine. *Chem. Commun.* **2010**, *46*, 5665–5667.
3. Zhang, M.; Qing, G.; Sun, T. Chiral Biointerface Materials. *Chem. Soc. Rev.* **2012**, *41*, 1972–1984.
4. Kunz, S.; Schreiber, P.; Ludwig, M.; Maturi, M. M.; Ackermann, O.; Tschurl, M.; Heiz, U. Rational Design, Characterization and Catalytic Application of Metal Clusters Functionalized with Hydrophilic, Chiral Ligands: A Proof of Principle Study. *Phys. Chem. Chem. Phys.* **2013**, *15*, 19253–19261.
5. Yasukawa, T.; Miyamura, H.; Kobayashi, S. Chiral Metal Nanoparticle-Catalyzed Asymmetric C-C Bond Formation Reactions. *Chem. Soc. Rev.* **2014**, *43*, 1450–1461.
6. Qi, H.; Hegmann, T. Formation of Periodic Stripe Patterns in Nematic Liquid Crystals Doped with Functionalized Gold Nanoparticles. *J. Mater. Chem.* **2006**, *16*, 4197–4205.
7. Qi, H.; O'Neil, J.; Hegmann, T. Chirality Transfer in Nematic Liquid Crystals Doped with (*S*)-Naproxen-Functionalized Gold Nanoclusters: An Induced Circular Dichroism Study. *J. Mater. Chem.* **2008**, *18*, 374–380.
8. Qi, H.; Hegmann, T. Postsynthesis Racemization and Place Exchange Reactions. Another Step to Unravel the Origin of Chirality for Chiral Ligand-Capped Gold Nanoparticles. *J. Am. Chem. Soc.* **2008**, *130*, 14201–14206.
9. Caligiuri, V.; De Sio, L.; Petti, L.; Capasso, R.; Rippa, M.; Maglione, M. G.; Tabiryan, N.; Umeton, C. Electro-/All-Optical Light Extraction in Gold Photonic Quasi-crystals Layered with Photosensitive Liquid Crystals. *Adv. Opt. Mater.* **2014**, *2*, 950–955.
10. Oh, H. S.; He, G. S.; Law, W.; Baev, A.; Jee, H.; Liu, X.; Urbas, A.; Lee, C.; Choi, B. L.; Swihart, M. T.; *et al.* Manipulating Nanoscale Interactions in a Polymer Nanocomposite for Chiral Control of Linear and Nonlinear Optical Functions. *Adv. Mater.* **2014**, *26*, 1607–1611.
11. Zhang, S.; Park, Y.; Li, J.; Lu, X.; Zhang, W.; Zhang, X. Negative Refractive Index in Chiral Metamaterials. *Phys. Rev. Lett.* **2009**, *102*, 023901.
12. Gautier, C.; Bürgi, T. Chiral Gold Nanoparticles. *ChemPhysChem* **2009**, *10*, 483–492.
13. Bürgi, T. Shining Light at Working Interfaces and Chiral Nanoparticles. *Chimia* **2011**, *65*, 157–167.
14. Shemer, G.; Krichevski, O.; Markovich, G.; Molotsky, T.; Lubitz, I.; Kotlyar, A. B. Chirality of Silver Nanoparticles Synthesized on DNA. *J. Am. Chem. Soc.* **2006**, *128*, 11006–11007.
15. Govorov, A. O.; Fan, Z.; Hernandez, P.; Slocik, J. M.; Naik, R. R. Theory of Circular Dichroism of Nanomaterials Comprising Chiral Molecules and Nanocrystals: Plasmon Enhancement, Dipole Interactions, and Dielectric Effects. *Nano Lett.* **2010**, *10*, 1374–1382.
16. Chen, W.; Bian, A.; Agarwal, A.; Liu, L.; Shen, H.; Wang, L.; Xu, C.; Kotov, N. A. Nanoparticle Superstructures Made by Polymerase Chain Reaction: Collective Interactions of Nanoparticles and a New Principle for Chiral Materials. *Nano Lett.* **2009**, *9*, 2153–2159.
17. Zhao, Y.; Xu, L.; Ma, W.; Wang, L.; Kuang, H.; Xu, C.; Kotov, N. A. Shell-Engineered Chiroplasmonic Assemblies of Nanoparticles for Zeptomolar DNA Detection. *Nano Lett.* **2014**, *14*, 3908–3913.
18. Guerrero-Martínez, A.; Auguié, B.; Alonso-Gómez, J. L.; Džolić, Z.; Gómez-Graña, S.; Žinić, M.; Cid, M. M.; Liz-Marzán, L. M. Intense Optical Activity from Three-Dimensional Chiral Ordering of Plasmonic Nanoantennas. *Angew. Chem., Int. Ed.* **2011**, *50*, 5499–5503.
19. Schaaff, T. G.; Whetten, R. L. Giant Gold-Glutathione Cluster Compounds: Intense Optical Activity in Metal-Based Transitions. *J. Phys. Chem. B* **2000**, *104*, 2630–2641.
20. Noguez, C.; Garzón, I. L. Optically Active Metal Nanoparticles. *Chem. Soc. Rev.* **2009**, *38*, 757–771.
21. Schaaff, T. G.; Knight, G.; Shafigullin, M. N.; Borkman, R. F.; Whetten, R. L. Isolation and Selected Properties of a 10.4 kDa Gold: Glutathione Cluster Compound. *J. Phys. Chem. B* **1998**, *102*, 10643–10646.
22. Jadzinsky, P. D.; Calero, G.; Ackerson, C. J.; Bushnell, D. A.; Kornberg, R. D. Structure of a Thiol Monolayer-Protected Gold Nanoparticle at 1.1 Å Resolution. *Science* **2007**, *318*, 430–433.
23. Negishi, Y.; Nobusada, K.; Tsukuda, T. Glutathione-Protected Gold Clusters Revisited: Bridging the Gap between Gold(I)-Thiolate Complexes and Thiolate-Protected Gold Nanocrystals. *J. Am. Chem. Soc.* **2005**, *127*, 5261–5270.
24. Gautier, C.; Bürgi, T. Chiral *N*-Isobutyryl-cysteine Protected Gold Nanoparticles: Preparation, Size Selection, and Optical Activity in the UV−Vis and Infrared. *J. Am. Chem. Soc.* **2006**, *128*, 11079–11087.
25. Knoppe, S.; Dharmaratne, A. C.; Schreiner, E.; Dass, A.; Bürgi, T. Ligand Exchange Reactions on Au_{38} and Au_{40} Clusters: A Combined Circular Dichroism and Mass Spectrometry Study. *J. Am. Chem. Soc.* **2010**, *132*, 16783–16789.
26. Knoppe, S.; Bürgi, T. Chirality in Thiolate-Protected Gold Clusters. *Acc. Chem. Res.* **2014**, *47*, 1318–1326.
27. Si, S.; Gautier, C.; Boudon, J.; Taras, R.; Gladiali, S.; Bürgi, T. Ligand Exchange on Au_{25} Cluster with Chiral Thiols. *J. Phys. Chem. C* **2009**, *113*, 12966–12969.
28. Santizo, I. E.; Hidalgo, F.; Pérez, L. A.; Noguez, C.; Garzón, I. L. Intrinsic Chirality in Bare Gold Nanoclusters: The Au_{34}^- Case. *J. Phys. Chem. C* **2008**, *112*, 17533–17539.
29. Guerrero-Martínez, A.; Alonso-Gómez, J. L.; Auguié, B.; Cid, M. M.; Liz-Marzán, L. M. From Individual to Collective Chirality in Metal Nanoparticles. *Nano Today* **2011**, *6*, 381–400.
30. Xia, Y.; Zhou, Y.; Tang, Z. Chiral Inorganic Nanoparticles: Origin, Optical Properties and Bioapplications. *Nanoscale* **2011**, *3*, 1374–1382.
31. Solladié, G.; Zimmermann, R. G. Liquid Crystals: A Tool for Studies on Chirality. *Angew. Chem., Int. Ed. Engl.* **1984**, *23*, 348–362.
32. Kitzerow, H.-S.; Bahr, C., Eds.; In *Chirality in Liquid Crystals (Partially Ordered Systems)*; Springer: New York, 2001; p 27.
33. Eelkema, R.; Feringa, B. L. Amplification of Chirality in Liquid Crystals. *Org. Biomol. Chem.* **2006**, *4*, 3729–3745.
34. Fasoli, H.; Echegoyen, L. E.; Hernandez, J. C.; Gokel, G. W.; Echegoyen, L. Evidence from E.S.R. Studies for Virtual Immobility in Niosomes Derived from Steroidal Lariat Ethers. *J. Chem. Soc., Chem. Commun.* **1989**, 578–580.
35. Leigh, W. J.; Mitchell, D. S. Organic Reactions in Liquid Crystalline Solvents. 6. Regiochemical Control of Bimolecular Chemical Reactivity in Smectic and Cholesteric Liquid Crystals. *J. Am. Chem. Soc.* **1988**, *110*, 1311–1313.
36. Shinkai, S.; Murata, K. Cholesterol-Based Functional Tectons as Versatile Building-Blocks for Liquid Crystals, Organic Gels and Monolayers. *J. Mater. Chem.* **1998**, *8*, 485–495.
37. Mulvaney, P. Surface Plasmon Spectroscopy of Nanosized Metal Particles. *Langmuir* **1996**, *12*, 788–800.
38. Link, S.; El-Sayed, M. Size and Temperature Dependence of the Plasmon Absorption of Colloidal Gold Nanoparticles. *J. Phys. Chem. B* **1999**, *103*, 4212–4217.
39. Terrill, R. H.; Postlethwaite, T. A.; Chen, C.; Poon, C.; Terzis, A.; Chen, A.; Hutchison, J. E.; Clark, M. R.; Wignall, G. Monolayers in Three Dimensions: NMR, SAXS, Thermal, and Electron Hopping Studies of Alkanethiol Stabilized Gold Clusters. *J. Am. Chem. Soc.* **1995**, *117*, 12537–12548.
40. Leff, D. V.; Ohara, P. C.; Heath, J. R.; Gelbart, W. M. Thermodynamic Control of Gold Nanocrystal Size: Experiment and Theory. *J. Phys. Chem.* **1995**, *99*, 7036–7041.
41. Nobusada, K. Electronic Structure and Photochemical Properties of a Monolayer-Protected Gold Cluster. *J. Phys. Chem. B* **2004**, *108*, 11904–11908.
42. Goldsmith, M.; George, C. B.; Zuber, G.; Naaman, R.; Waldeck, D. H.; Wipf, P.; Beratan, D. N. The Chiroptical Signature of Achiral Metal Clusters Induced by Dissymmetric Adsorbates. *Phys. Chem. Chem. Phys.* **2006**, *8*, 63–67.
43. Yao, H.; Fukui, T.; Kimura, K. Chiroptical Responses of D-/L-Penicillamine-Capped Gold Clusters under Perturbations of Temperature Change and Phase Transfer. *J. Phys. Chem. C* **2007**, *111*, 14968–14976.

44. Govorov, A. O. Plasmon-Induced Circular Dichroism of a Chiral Molecule in the Vicinity of Metal Nanocrystals. Application to Various Geometries. *J. Phys. Chem. C* **2011**, *115*, 7914–7923.
45. Lieberman, I.; Shemer, G.; Fried, T.; Kosower, E.; Markovich, G. Plasmon-Resonance-Enhanced Absorption and Circular Dichroism. *Angew. Chem., Int. Ed.* **2008**, *47*, 4855–4857.
46. Gerard, V. A.; Gun'ko, Y. K.; Defrancq, E.; Govorov, A. O. Plasmon-Induced CD Response of Oligonucleotide-Conjugated Metal Nanoparticles. *Chem. Commun.* **2011**, *47*, 7383–7385.
47. Govorov, A. O.; Gun'ko, Y. K.; Slocik, J. M.; Gerard, V. A.; Fan, Z.; Naik, R. R. Chiral Nanoparticle Assemblies: Circular Dichroism, Plasmonic Interactions, and Exciton Effects. *J. Mater. Chem.* **2011**, *21*, 16806–16818.
48. Knoppe, S.; Dharmaratne, A. C.; Schreiner, E.; Dass, A.; Bürgi, T. Ligand Exchange Reactions on Au_{38} and Au_{40} Clusters: A Combined Circular Dichroism and Mass Spectrometry Study. *J. Am. Chem. Soc.* **2010**, *132*, 16783–16789.
49. Tang, Z.; Ahuja, T.; Wang, S.; Wang, G. Near Infrared Luminescence of Gold Nanoclusters Affected by the Bonding of 1,4-Dithiolate Durene and Monothiolate Phenylethanethiolate. *Nanoscale* **2012**, *4*, 4119–4124.
50. Meng, X.; Xu, Q.; Wang, S.; Zhu, M. Ligand-Exchange Synthesis of Selenophenolate-Capped Au25 Nanoclusters. *Nanoscale* **2012**, *4*, 4161–4165.
51. Saeva, F. D.; Olin, G. R. Extrinsic Circular Dichroism in Twisted Nematic Mesophases. *J. Am. Chem. Soc.* **1976**, *98*, 2709–2711.
52. Mirzaei, J.; Urbanski, M.; Yu, K.; Kitzerow, H.- S.; Hegmann, T. Nanocomposites of a Nematic Liquid Crystal Doped with Magic-Sized CdSe Quantum Dots. *J. Mater. Chem.* **2011**, *21*, 12710–12716.
53. Qi, H.; Kinkead, B.; Hegmann, T. Unprecedented Dual Alignment Mode and Freedericksz Transition in Planar Nematic Liquid Crystal Cells Doped with Gold Nanoclusters. *Adv. Funct. Mater.* **2008**, *18*, 212–221.
54. Kinkead, B.; Hegmann, T. Effects Of Size, Capping Agent, and Concentration of CdSe and CdTe Quantum Dots Doped into a Nematic Liquid Crystal on the Optical and Electro-Optic Properties of the Final Colloidal Liquid Crystal Mixture. *J. Mater. Chem.* **2010**, *20*, 448–458.
55. Mirzaei, J.; Urbanski, M.; Kitzerow, H.-S.; Hegmann, T. Hydrophobic Gold Nanoparticles *via* Silane Conjugation: Chemically and Thermally Robust Nanoparticles as Dopants for Nematic Liquid Crystals. *Philos. Trans. R. Soc., A* **2013**, *371*, 1471–2962.
56. Mirzaei, J.; Urbanski, M.; Kitzerow, H.-S; Hegmann, T. Synthesis of Liquid Crystal Silane-Functionalized Gold Nanoparticles and Their Effects on the Optical and Electro-Optic Properties of a Structurally Related Nematic Liquid Crystal. *ChemPhysChem* **2014**, *15*, 1381–1391.
57. Kosa, T.; Bodnar, V. H.; Taheri, B.; Palffy-Muhoray, P. Accurate Measurement of the Helical Twisting Power of Chiral Dopants. *Mol. Cryst. Liq. Cryst.* **2001**, *369*, 129–137.
58. Schubert, C. P. J.; Tamba, M. G.; Mehl, G. H. Chiral Nematic Organo-Siloxane Oligopodes Based on an Axially Chiral Binaphthalene Core. *Chem. Commun.* **2012**, *48*, 6851–6853.
59. Krishnamurthy, S.; Chen, S. H. A Comparative Study of Helical Sense and Twisting Power in Low-Molar-Mass and Polymeric Chiral Nematics. *Macromolecules* **1992**, *25*, 4485–4489.
60. Qi, H.; Kinkead, B.; Hegmann, T. Effect of Functionalized Metal and Semiconductor Nanoparticles in Nematic Liquid Crystal Phases. *Proc. SPIE-Int. Soc. Opt. Eng.* **2008**, *6911*, 691106.
61. Yang, A.; Wang, B.; Cui, D.; Kerwood, D.; Wilkens, S.; Han, J.; Luk, Y.-Y. Stereochemical Control of Nonamphiphilic Lyotropic Liquid Crystals: Chiral Nematic Phase of Assemblies Separated by Six Nanometers of Aqueous Solvents. *J. Phys. Chem. B* **2013**, *117*, 7133–7143.
62. Bruckner, J. R.; Porada, J. H.; Dietrich, C. F.; Dierking, I.; Giesselmann, F. A Lyotropic Chiral Smectic C Liquid Crystal with Polar Electrooptic Switching. *Angew. Chem., Int. Ed.* **2013**, *52*, 8934–8937.
63. Reznikov, M.; Sharma, A.; Hegmann, T. Ink-Jet Printed Nanoparticle Alignment Layers: Easy Design and Fabrication of Patterned Alignment Layers for Nematic Liquid Crystals. *Part. Part. Syst. Charact.* **2014**, *31*, 257–265.
64. Gvozdovskyy, I.; Jampani, V. S. R.; Škarabot, M.; Muševič, I. Light-Induced Rewiring and Winding of Saturn Ring Defects in Photosensitive Chiral Nematic Colloids. *Eur. Phys. J. E* **2013**, *36*, 1–8.
65. Kasyanyuk, D.; Slyusarenko, K.; West, J.; Vasnetsov, M.; Reznikov, Y. Formation of Liquid-Crystal Cholesteric Pitch in the Centimeter Range. *Phys. Rev. E* **2014**, *89*, 022503.